Locking-free Mixed Finite Element Methods and their Spurious Hourglassing Patterns

Moritz Hille[1], Robin Pfefferkorn[1] and Peter Betsch[1*]
[1]Institute of Mechanics, Karlsruhe Institute of Technology (KIT), Germany

This is a preprint of the following chapter: Hille, M., Pfefferkorn, R., and Betsch, P., "Locking-free Mixed Finite Element Methods and their Spurious Hourglassing Patterns", published in *Current Trends and Open Problems in Computational Mechanics*, edited by Aldakheel, F., Hudobivnik, B., Soleimani, M., Wessels, H., Weissenfels, C., and Marino M., 2022, Springer reproduced with permission of Springer Nature Switzerland AG. The final authenticated version is available online at: `https://dx.doi.org/10.1007/978-3-030-87312-7_19`

03.12.2020

We present the five field mixed finite element formulation introduced by Armero and extend it to 3D problems. It combines the nonlinear mixed pressure element with an enhanced assumed strain (EAS) method based on the transposed Wilson modes. The well-known mixed pressure element arises from a Hu-Washizu-like variational principle, where dilatation and pressure are independent variables. This functional is further modified using the EAS framework to get the mixed formulation presented in this work. The element is compared to several mixed pressure and EAS element formulations showing its great performance in alleviating volumetric and shear locking in large deformation problems. The main focus of the present work is spurious hourglassing of mixed finite elements that arise in hyperelastic and elasto-plastic simulations.

Keywords: mixed finite elements, enhanced assumed strain, hyperelasticity, elasto-plasticity, robustness, numerical instabilities.

1 Introduction

The finite element method (FEM) (see e.g. Wriggers [19]) is one of the most significant methods to numerically solve partial differential equations (PDE) in solid continuum mechanics. Its key idea is to subdivide a body in the name giving finite elements (FE) and to approximate the deformation of this body using the weak form of a PDE.

One of the major phenomenons that limits the applicability of low-order displacement elements is locking, which denotes numerical stiffening of the body. It causes too small deformations and slow convergence with mesh refinement. A distinction is made between shear and volumetric

* Corresponding author: Peter.Betsch@kit.edu

locking occurring in bending dominated problems and in the incompressible limit, respectively. In 1985 Simo et al. [14] presented a mixed element formulation based on a Hu-Washizu [17] three field functional introducing extra variables for dilatation and pressure, such that the deviatoric and volumetric part of the strain tensor can be treated separately. This alleviates the effects of volumetric locking for nearly incompressible materials.

In 1990 and 1992 Simo and Rifai [13] and Simo and Armero [11] presented another widely used mixed finite element method called enhanced assumed strain method (EAS) for linear and non-linear deformations, respectively. This method introduced enhanced strains in addition to the compatible strains with ansatz functions based on the previously introduced popular incompatible displacement modes (see Wilson [18]). While EAS elements work extremely well for small deformation problems, they unfortunately suffer from spurious hourglassing instabilities under large deformation compression as first pointed out by Wriggers and Reese [20]. A first remedy to this problem was proposed by Korelc and Wriggers [6] who introduced a method of transposed Wilson modes in 1996 solving this problem for polyconvex elastic materials. However, the method proposed in Korelc and Wriggers [6] is not frame-invariant if it is subject to large rotations which was corrected by Glaser and Armero [3]. For more details on the long history of EAS elements, including various ansatz functions and transformations, see e.g. Pfefferkorn and Betsch [7]. Even though the transposed Wilson-modes eliminated hourglassing in hyperelastic problems, the element still suffers from hourglassing in elasto-plastic simulations. To the best knowledge of the authors, there exists no EAS element that overcomes this problem without introducing unphysical expressions with parameters to be set by the user.

In this paper we discuss an element formulation presented by Armero [1] in 2000, that combines the mixed pressure formulation of Simo et al. [14] with the EAS method of Glaser and Armero [3]. The key idea is to enhance only the non-diagonal elements of the deformation gradient yielding a specific enhancement of the deviatoric part of the strain tensor, since the locking of the volumetric part is taken care of by the mixed pressure ansatz. This yields a five field variational functional which is basis for a stable and hourglassing-free finite element method for nonlinear elastic material behavior with great results in computing deformations of hyperelastic as well as in elasto-plastic formulations. Most remarkably, the element presented by Armero [1] shows no hourglassing in 2D elasto-plastic simulations. Hence Armero [1] remedies the shear locking of the mixed pressure element of Simo et al. [14] whilst circumventing the spurious hourglassing effects of the EAS formulation by Simo and Armero [11] in 2D. The 3D case, however, has not been covered so far. In this paper we present a 3D version of this element formulation and provide numerical tests for 3D elastic and plastic material behavior. We show most importantly that, unfortunately, the 3D formulation of this element is not hourglassing-free in elasto-plastic simulations.

The paper is structured into four chapters. Chapter 2 covers the mixed finite element method of Armero [1]. Chapter 3 contains numerical tests assessing the performance and stability of the mixed element presented in Chapter 2 by comparing it to mixed EAS and mixed pressure element formulations. It is shown that the mixed pressure EAS element has extremely high robustness (concerning number of load steps and number of Newton-Raphson (NR) iterations) and is not susceptible to locking. However, in 3D it is not hourglassing-free in standard tests. Finally, Chapter 4 concludes the paper and its results with a short summary.

2 The Five-Field Finite Element Formulation

In this section we give an overview of the five-field finite element formulation, which was first presented by Armero [1] for 2D problems. In the present work we focus on the 3D formulation.

2.1 Deformation Gradient

We first introduce the deformation gradient $\mathbf{F}$ since its structure is the key to both mixed methods on which the present element relies. It combines the volumetric and deviatoric split used for the mixed pressure element in Simo et al. [14] with an additive enhancement. The purely displacement based deformation gradient

$$\mathbf{F}_\varphi(\boldsymbol{\varphi}) = \mathrm{Grad}\,(\boldsymbol{\varphi}) = \frac{\partial \boldsymbol{\varphi}(\mathbf{X})}{\partial \mathbf{X}} \tag{1}$$

is modified in the form

$$\mathbf{F}(\boldsymbol{\varphi}, \theta, \boldsymbol{\Gamma}) = \theta^{1/3} \widehat{J}^{-1/3} \widehat{\mathbf{F}}. \tag{2}$$

Therein, θ is the (independent) dilatation and $\widehat{J} = \det(\widehat{\mathbf{F}})$. Moreover, the enhancement is denoted by $(\widehat{\bullet})$ and the enhanced deformation gradient $\widehat{\mathbf{F}}$ is given by

$$\widehat{\mathbf{F}}(\boldsymbol{\varphi}, \boldsymbol{\Gamma}) = \mathbf{F}_\varphi(\boldsymbol{\varphi}) + \widetilde{\mathbf{F}}(\boldsymbol{\varphi}, \boldsymbol{\Gamma}), \tag{3}$$

where

$$\widetilde{\mathbf{F}}(\boldsymbol{\varphi}, \boldsymbol{\Gamma}) = \mathbf{F}_{\varphi,0}(\boldsymbol{\varphi}) \mathbf{F}_\Gamma(\boldsymbol{\Gamma}) \tag{4}$$

is the enhanced part of the deformation gradient, which depends apart from the enhanced degrees of freedom $\boldsymbol{\Gamma}$ on the deformations $\boldsymbol{\varphi}$ via $\mathbf{F}_{\varphi,0}$, which is the compatible deformation gradient (1) evaluated at the element centroid, in order to ensure frame invariance (see Simo et al. [12] and Glaser and Armero [3]). Finally, $\mathbf{F}_\Gamma$ includes the enhanced degrees of freedom Γ_i arranged in vector $\boldsymbol{\Gamma}$ and is specified in section 2.3.

2.2 Variational Framework

The classic variational potential for the pure displacement element formulation is extended by two constraints. The first condition on kinematic level, $J = \theta$ with $J = \det(\mathbf{F}_\varphi)$, is enforced by the Lagrange multiplier p in analogy to Simo et al. [14]. The second constraint ensures that the enhanced part of the deformation gradient $\widetilde{\mathbf{F}}$ vanishes on the continuum level and is enforced by the second Lagrange multiplier $\mathbf{P}$. This yields the five-field functional

$$\Pi(\boldsymbol{\varphi}, \theta, p, \boldsymbol{\Gamma}, \mathbf{P}) = \int_{\mathcal{B}_0} \left[W(\mathbf{C}) + p\,(J - \theta) - \mathbf{P} : \widetilde{\mathbf{F}} \right] \mathrm{d}V + \Pi_{\mathrm{ext}}(\boldsymbol{\varphi})\,, \tag{5}$$

where W is an arbitrary hyperelastic strain-energy function characterizing the behavior of body $\mathcal{B}$, which is mapped from its reference configuration $\mathcal{B}_0$ to its current configuration by deformation map $\boldsymbol{\varphi}$. Furthermore, Π_{ext} denotes the potential of external forces not further specified here and $\mathbf{C} = \mathbf{F}^{\mathrm{T}}\mathbf{F}$ is the modified Cauchy-Green tensor computed using $\mathbf{F}(\boldsymbol{\varphi}, \boldsymbol{\Gamma})$.

The five independent fields in (5) require the five stationary conditions

$$\delta_\varphi \Pi \;=\; \int_{\mathcal{B}_0} \mathrm{dev}(\boldsymbol{\tau}) : \widehat{\nabla}^{\mathrm{s}}(\delta\boldsymbol{\varphi}) + pJ\mathbf{I} : \nabla^{\mathrm{s}}(\delta\boldsymbol{\varphi}) - \delta_\varphi \widetilde{\mathbf{F}} : \mathbf{P}\ \mathrm{d}V + \delta_\varphi \Pi_{\mathrm{ext}} = 0, \tag{6a}$$

$$\delta_\theta \Pi = \int_{\mathcal{B}_0} \left(\frac{1}{3} \mathrm{tr}(\boldsymbol{\tau}) \theta^{-1} - p \right) \delta\theta \, \mathrm{d}V = 0, \tag{6b}$$

$$\delta_p \Pi = \int_{\mathcal{B}_0} \delta p \, (J - \theta) \, \mathrm{d}V = 0, \tag{6c}$$

$$\delta_\Gamma \Pi = \int_{\mathcal{B}_0} \mathrm{dev}(\boldsymbol{\tau}) : \mathrm{sym}\Big(\mathbf{F}_{\varphi,0} \delta_\Gamma \mathbf{F}_\Gamma \widehat{\mathbf{F}}^{-1} \Big) - \delta_\Gamma \widetilde{\mathbf{F}} : \mathbf{P} \, \mathrm{d}V = 0, \tag{6d}$$

$$\delta_P \Pi = -\int_{\mathcal{B}_0} \delta \mathbf{P} : \widetilde{\mathbf{F}} \, \mathrm{d}V = 0, \tag{6e}$$

where $\boldsymbol{\tau}$ is the constitutive Kirchhoff stress tensor and assumes the usual form

$$\boldsymbol{\tau} = \mathbf{F}\mathbf{S}\mathbf{F}^{\mathrm{T}} \quad \text{with} \quad \mathbf{S} = 2 \frac{\partial W(\mathbf{C})}{\partial \mathbf{C}} \tag{7}$$

for a hyperelastic material model[1]. Furthermore, $\widehat{\nabla}^{\mathrm{s}}(\bullet)$ is a modified symmetric gradient in the spatial configuration that arises from the derivative of the Cauchy-Green tensor $\mathbf{C}$ with respect to $\boldsymbol{\varphi}$. The modified gradient $\widehat{\nabla}(\bullet)$ is given by

$$\widehat{\nabla}(\bullet) := \widehat{\nabla}_{\mathbf{x}}(\bullet) = \Big[\nabla_{\mathbf{X}}(\bullet) + \mathbf{F}_\Gamma^{\mathrm{T}} \nabla_{\mathbf{0}}(\bullet) \Big] \widehat{\mathbf{F}}^{-1}, \tag{8}$$

where $\nabla_{\mathbf{0}}(\bullet) = \nabla_{\mathbf{X}}(\bullet)\Big|_{\xi=\mathbf{0}}$ and $\nabla_{\mathbf{X}}(\bullet) = \mathrm{Grad}(\bullet)$.

2.3 Discretization

For all simulations we consider the common isoparametric concept and the Bubnov-Galerkin method. Thus, the approximate $(\bullet)^{\mathrm{h}}$ and elementwise $(\bullet)^e$ position $\mathbf{X}^{\mathrm{h},e}$ and displacement $\boldsymbol{\varphi}^{\mathrm{h},e}$ as well as its variation $\delta\boldsymbol{\varphi}^{\mathrm{h},e}$ are given by

$$\mathbf{X}^{\mathrm{h},e} = \sum_{I \in \mathcal{I}} N_I^e \mathbf{X}_I^e, \quad \boldsymbol{\varphi}^{\mathrm{h},e} = \sum_{I \in \mathcal{I}} N_I^e \boldsymbol{\varphi}_I^e \quad \text{and} \quad \delta\boldsymbol{\varphi}^{\mathrm{h},e} = \sum_{I \in \mathcal{I}} N_I^e \delta\boldsymbol{\varphi}_I^e \tag{9}$$

for all elements $e \in \{1, 2, \ldots, n_e\}$ in the subdivision $\mathcal{B}_0^{\mathrm{h}} = \bigcup_{e=1}^{n_e} \Omega^e$ of body $\mathcal{B}_0$. Furthermore, $\mathcal{I}$ is the set of nodes in the reference element $\Omega_\square$. The standard trilinear Lagrangian shape functions for the eight noded cube are employed.

Constant ansatz functions are used for the dilatation θ and Lagrange multiplier p since they match well with linear shape functions on the deformation $\boldsymbol{\varphi}$ if θ and p are restricted to each element Ω^e as discussed e.g. in Hughes [4]. This yields

$$\theta^{\mathrm{h},e} = \mathrm{const} \quad \text{and} \quad p^{\mathrm{h},e} = \mathrm{const} \quad \text{in every element.} \tag{10}$$

This element does not fulfill the LBB-condition (cf. Boffi et al. [2]). This means, that for some boundary conditions checkerboard solutions for the aproximated pressure arises. Fortunately, this can easily be fixed by various workarounds e.g. $\mathcal{L}^2$-smoothing (cf. Wriggers [19]).

Finally, we discuss the approximation of $\mathbf{F}_\Gamma(\boldsymbol{\Gamma})$ introduced in (4). Armero [1] uses transposed Wilson modes which are first described in the work of Korelc and Wriggers [6]. The basic idea of the element proposed by Armero [1] is to only use the non-diagonal modes.[2] We extend this

[1] Note that all terms in (6) refer to the spatial configuration except for terms containing $\mathbf{P}$ or $\delta\mathbf{P}$ since these terms vanish on discrete level due to the orthogonality condition given below.

[2] We also tested the same element with all nine transposed Wilson Modes for the enhanced field. That element is even softer than the element of Armero, which is too soft in pure bending problems with undistorted meshes. Thus, the element with all 9 enhanced modes is not taken into account in subsequent investigations.

formulation to the three-dimensional space which yields an enhancement field of the form

$$\mathbf{F}_\Gamma(\boldsymbol{\Gamma}^e) = \frac{j_0^{\mathrm{h},e}}{j^{\mathrm{h},e}(\boldsymbol{\xi})} \left(\mathbf{J}_0^{\mathrm{h},e}\right)^{-\mathrm{T}} \left(\begin{bmatrix} 0 & \Gamma_1^e\xi & \Gamma_2^e\xi \\ \Gamma_3^e\eta & 0 & \Gamma_4^e\eta \\ \Gamma_5^e\zeta & \Gamma_6^e\zeta & 0 \end{bmatrix} \right) \left(\mathbf{J}_0^{\mathrm{h},e}\right)^{-1}, \tag{11}$$

where $\mathbf{J}_0 = \mathbf{J}\Big|_{\xi=\mathbf{0}}$ and $\mathbf{J}$ is the Jacobian matrix of the isoparametric map. Analogously, their determinants are given by $j = \det(\mathbf{J})$ and $j_0 = \det(\mathbf{J})\Big|_{\xi=\mathbf{0}}$, respectively.

In analogy to standard EAS elements the present five-field element formulation fulfills the patch test provided that $\int_{\Omega_\square} \mathbf{F}_\Gamma \, \mathrm{d}\Omega_\square = 0$ is fulfilled (see Armero [1]).

The usual $\mathcal{L}^2$-orthogonality condition assumed between discrete stress and strain field yields

$$\int_{\Omega^e} \widetilde{\mathbf{F}}^{\mathrm{h},e} : \delta\mathbf{P}^{\mathrm{h},e} \, \mathrm{d}V = \int_{\Omega^e} \delta\widetilde{\mathbf{F}}^{\mathrm{h},e} : \mathbf{P}^{\mathrm{h},e} \, \mathrm{d}V = 0 \tag{12}$$

on element level. This allows to eliminate $\mathbf{P}$ in the discrete case such that only four fields remain in the discretized version of functional (5).

3 Numerical Investigations

This chapter covers benchmarks testing the performance of the finite element formulation presented in Section 2. The element is compared to the standard isoparametric displacement element and popular (well-working) mixed elements. Armero [1] already described and evaluated the mixed pressure EAS element using various 2D tests. Thus, the focus of this work lies on the 3D formulation.

The element proposed by Armero is denoted Q1/P0ET2. Its 3D extension covered in this work is named H1/P0ET6. The 3D elements used for comparison in the following numerical examples are:

- H1, the standard isoparametric 8-node displacement element,
- H1/E9, the classic EAS element formulation (see Simo and Armero [11]) and H1/ET9, the EAS formulation with transposed Wilson modes (see Glaser and Armero [3]),
- HA1/ET12, an extension of H1/ET9 with additional volumetric modes using a 9-point integration (see Pfefferkorn and Betsch [7]) and
- H1/E9-MIP and HA1/E12-MIP the EAS elements with improved robustness by use of the mixed integration point (MIP) method (see Pfefferkorn et al. [9]),
- H1/P0, the three field mixed pressure element (see Simo et al. [14]) and
- H1/S18, the well known assumed stress element by Pian and Sumihara [10], which has 18 stress modes in 3D.

We consider two material models for all simulations. First, the nonlinear neo-Hookean material model with strain-energy function

$$W = \frac{\mu}{2}(\mathrm{tr}(\mathbf{C}) - 3) + \frac{\lambda}{2}(\ln J)^2 - \mu \ln J \tag{13}$$

for elastic behavior.[3][4] Second, the multiplicative J_2-plasticity model with nonlinear isotropic hardening and the Hencky elastic law as proposed by e.g. Simo [15]. The material parameters of that model are set to their usual values (see e.g. [1], [3] or [8]).

3.1 Cooks Membrane

The first test described in the present work is the Cooks membrane test. Figure 1 shows the system, which is clamped on the left. We employ the elastic model given in (13) with material parameters $\mu = 756.00$ and $\lambda = 8.2669 \cdot 10^4$.

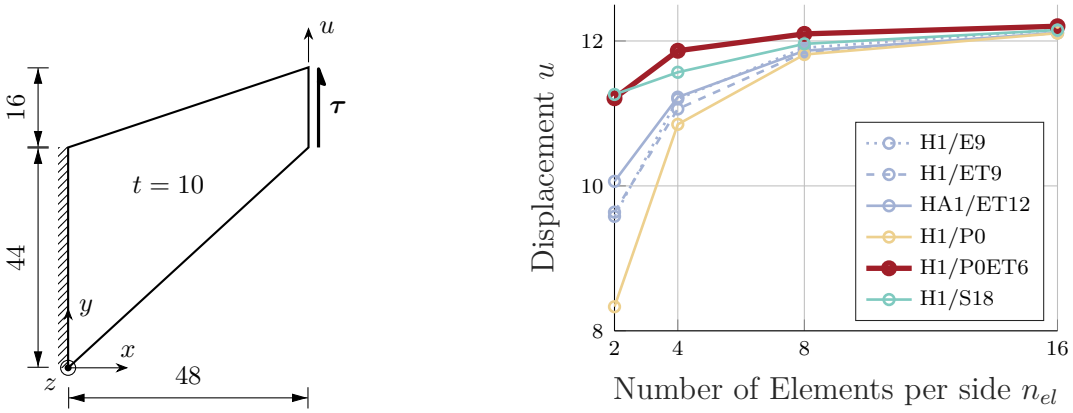

Figure 1: Cooks membrane: system (left) and displacement u of the hindmost node in the right upper corner (right).

The focus of this test is on shear and volumetric locking. To determine the elements performance, we evaluate the displacement u in y-direction of the top right corner caused by equally distributed shear stress $\boldsymbol{\tau} = 100$. The right image in Figure 1 shows this deformation in dependence of the number of elements per side for the various mixed elements (there are always 2 elements in direction of the thickness).

The worst element is H1/P0 which suffers from shear locking since only the volumetric parts are modified in this formulation. On the other end, H1/P0ET6 exhibits the best results with fastest convergence with mesh refinement.

Another interesting result of this investigation is the number of load steps required to achieve convergence of Newton's method. Regardless of the mesh size, H1/P0, H1/S18 and H1/P0ET6 only need one load step for convergence while EAS elements need at least six load steps.[5] This suggests, that H1/P0ET6 inherits the robustness, meaning size of applicable load steps and number of necessary Newton iterations, from H1/P0. Consequently, it is numerically more efficient. This result is confirmed in Section 3.5. Note that the efficiency strongly depends on the aspect ratio of the elements in case of H1/P0ET6.

[3] Note that no volumetric deviatoric split in W (13) is considered in the present work in contrast to many works on mixed elements with approximation of the pressure (see e.g. Simo et. al [14]).

[4] A inverse stress strain relation of (13) for H1/S18 is given in [9].

[5] Elements with MIP method need even slightly more iterations in this example, which shows that there are cases where this method is not advantageous. Nevertheless, it improves convergence in many cases (see Pfefferkorn et al. [9]).

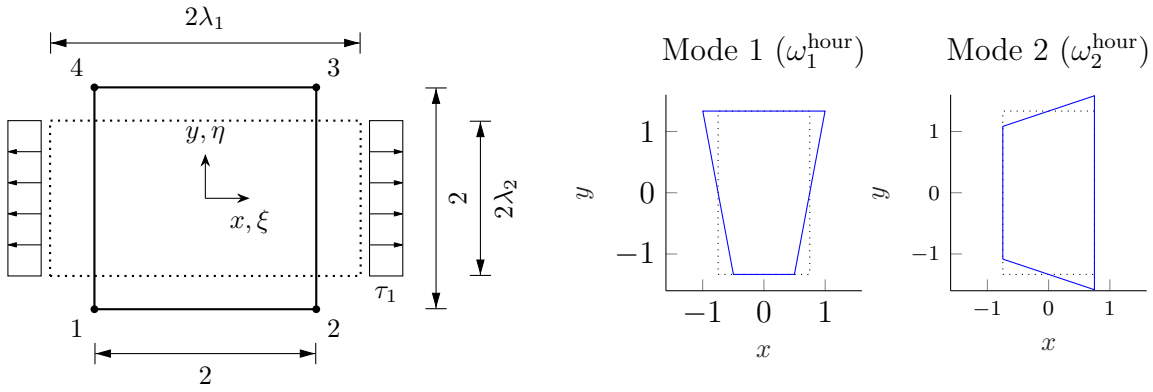

Figure 2: Setup for stability test 2D (left) and hourglass modes 2D (right).

3.2 Stability Test

This section describes the modal analysis presented in Armero [1], where the eigenvalues of the stiffness matrix are evaluated to examine possible instabilities from so called hourglass modes. Armero [1] covers the 2D version of this test while this paper focuses on 3D testing as mentioned above.

Every eigenpair linked to an eigenvalue ω_i of the element stiffness matrix denotes a specific mode, that describes one kind of motion or deformation, that the element can perform. Besides the six rigid body and the six constant strain modes, there are twelve hourglass modes in 3D with a corresponding eigenvalue ω_i^{hour}. These eigenvalues can cause locking and numerical instabilities and sometimes yield non-physical deformations in numerical computations. Negative hourglass eigenvalues can cause typical hourglass patterns, thus, the construction of element formulations that exhibit only positive eigenvalues should be the goal.

For the 3D version of this test we consider a single finite element $\Omega^e = [-1, 1]^3$. It is deformed in a state of uniaxial stress which allows to analytically compute the principal stretch $\lambda_2 = \lambda_3$ for any given λ_1 using conditions $\tau_2 = \tau_3 = 0$.[6] Armero [1] showed, that for the plane strain case of the problem depicted in Figure 2, the hourglass-eigenvectors are always constant and thus let us readily compute the corresponding eigenvalues. In the uniaxial 3D case, the hourglass-eigenvectors depend on the stiffness matrix and thus on the material properties and the element formulation. However, they can still be computed analytically as shown in Pfefferkorn and Betsch [8].

Since the eigenmodes are well known, a matrix of eigenvectors can be described and a product of the stiffness matrix and the hourglass matrix yields the eigenvalues. For the elastic case we use the Lamé parameters $\lambda = 10^5$ and $\mu = 20$.

Before we list the 3D results, we give a brief summary of previous results for 2D elements. The first thorough work on the instabilities under compression of Q1/E4 is Wriggers and Reese [20]. Viehbahn et al. [16] showed for Q1/S5 and Wriggers and Reese [20] for Q1/E4, that these two elements show instabilities in uniaxial pressure ($\omega_2^{\text{hour}} < 0$ for $\lambda_1 < 1$).[7] All other elements

[6] Due to the non-linearity of this expression a solver e.g. Newton's method might be required to solve for λ_2. However, for the considered material models, an analytic solution is possible.

[7] Q1/S5 has a different behavior in tension than all other elements which might emerge from problems with the Legendre transformation.

tested exhibit no negative hourglass eigenvalues as shown by Armero [1]. In the case of the elasto-plastic material model only Q1/E4 shows instabilities in uniaxial pressure while all other EAS elements suffer from instabilities under tension (see also Section 3.3).

There are twelve hourglass eigenvalues in the three-dimensional case. Due to symmetry of the uniaxial stress problem, some of these twelve modes are identical except for a rotation around the x-axis (see Pfefferkorn and Betsch [8]). Thus, only the unique eigenvalues are shown in Figure 3 for the neo-Hookean and for the elasto-plastic material model, respectively.

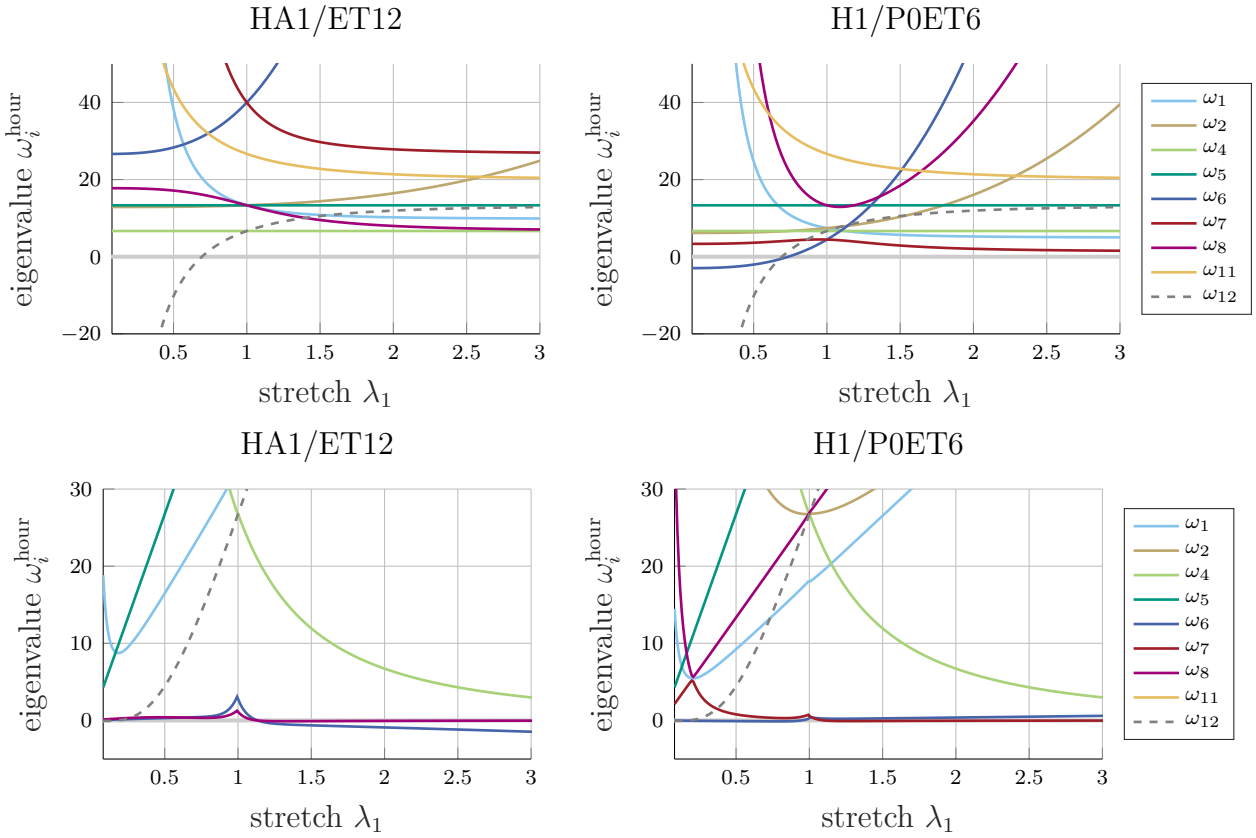

Figure 3: Hourglass eigenvalues of 3D elements for the neo-Hookean (top) and elasto-plastic (bottom) material model.

For the elastic material behavior mode 6 of Q1/P0ET6 is slightly negative under compression although this seems not to influence its stability in practical simulations.

For the plastic material behavior Q1/P0 shows the best results since all eigenvalues are strictly positive. H1/E9, HA1/ET12 and H1/P0ET6 all have instabilities in the plastic case since various eigenvalues are below zero. In particular, modes 7 and 8 have different shapes and much lower values for H1/P0ET6 than for standard EAS elements. This ultimately leads to the hourglassing patterns observed in Section 3.4. The EAS elements exhibit negative modes as well. In particular, ω_6^{hour} is negative. However, this mode is not activated in distorted meshes as shown in Sec 3.4, whereas it leads to hourglassing situations in plane strain necking problems (see Section 3.3).

3.3 Necking Plane Strain

In this and the following example we consider a necking simulation using the elasto-plastic material and focus on hourglassing patterns. A rectangular bar with a length of $L = 53.334$ and a width of $R = 12.826$ is subject to prescribed displacements $\bar{v}$. Necking is initiated by a geometric imperfection in form of a linear reduction of R to $\bar{R}$ by ΔR. In order to capture the hourglassing patterns, a total of 200 load steps is considered to reach $\bar{v} = 7$. Note that only one fourth of the specimen needs to be simulated due to symmetry. For more details see e.g. Armero [1] or Pfefferkorn and Betsch [8].

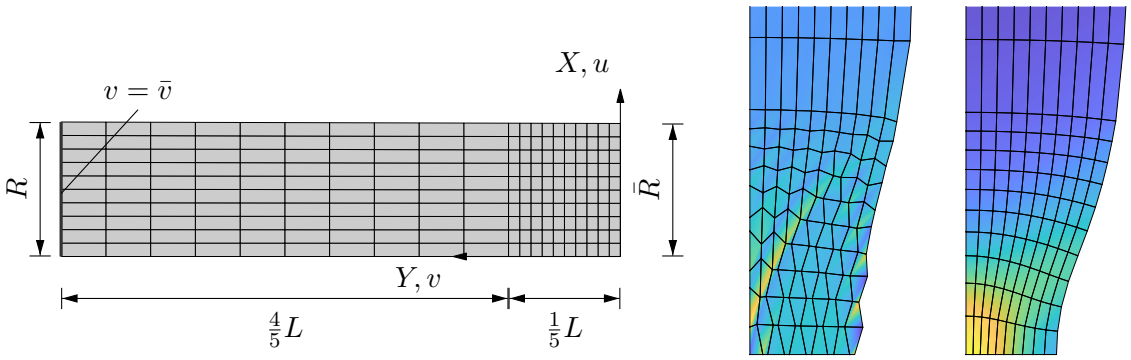

Figure 4: Thin bar: setup (left) and deformed mesh for $\bar{v} = 5.6$ of Q1/ET4 (middle) and Q1/P0ET2 (right).

As shown in Figure 4, exemplary for Q1/ET4, all EAS based element formulations suffer from hourglassing patterns while Q1/P0 and Q1/P0ET2 are hourglassing-free. Here, the negative eigenvalues of Mode 6 (or rather its 2D equivalent) observed in Section 3.2 cause the hourglassing patterns.

3.4 Necking Circular Bar

In analogy to Section 3.3, the 3D version of the necking problem is conducted on one eighth of a circular bar of length $L = 53.334$ and Radius $R = 6.413$. After a total of 50 load steps opposite results to Section 3.3 are obtained as shown in Figure 5. All EAS based elements are hourglassing-free, but the element of Armero, H1/P0ET6, shows hourglassing patterns. In dissent to the results of Simo and Armero [11] H1/P0 is hourglassing-free. Thus, for the current problem with its distorted elements, the negative Mode 6 does not seem to induce hourglassing while the negative modes 7 and 8 observed for H1/P0ET6 induce hourglassing.

3.5 Spherical Shell with Opening

The final test presented in the present paper is the spherical shell problem with opening modeled using the neo-Hookean nonlinear elastic material model with $\lambda = 1.2115 \cdot 10^5$ and $\mu = 8.0769 \cdot 10^4$. The left image in Figure 6 shows the setup with middle radius $r = 10$, thickness 0.5 and opening angle $\beta = 18°$ while the right image shows the deformed mesh computed with element formulation H1/E9. The shell is deformed by prescribed displacements applied at the inner edge of the top opening. For more details on setup and procedure see e.g. Korelc et al. [5].

Table 1 presents the required number of load steps n_{steps} and total number of Newton-Raphson (NR) iterations n_{NR} plus the resulting reaction force in z-direction R_z.[8] Since the aspect ratio

[8] We use the Newton tolerance $||R|| < 1 \cdot 10^{-8}$ as well as a maximum of 20 numerical iterations per load step.

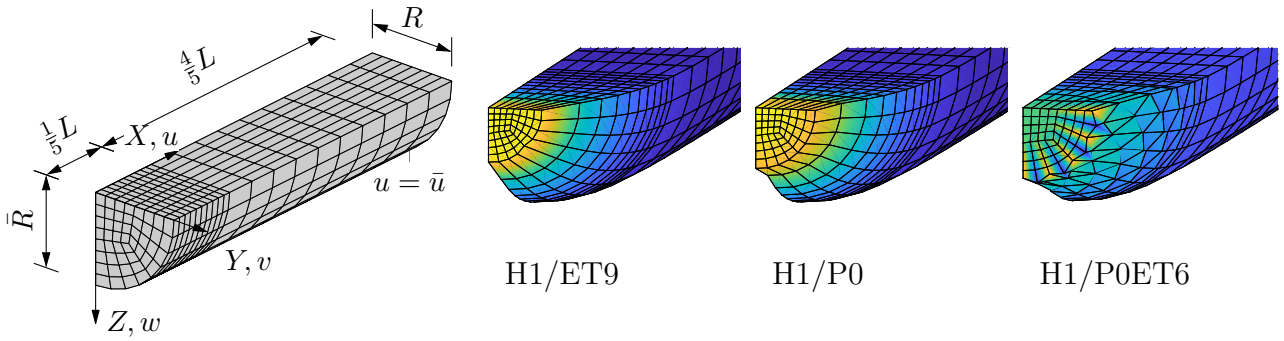

Figure 5: Circular bar: setup (left) and from left to right the deformed meshes of H1/ET9, H1/P0 and H1/P0ET6.

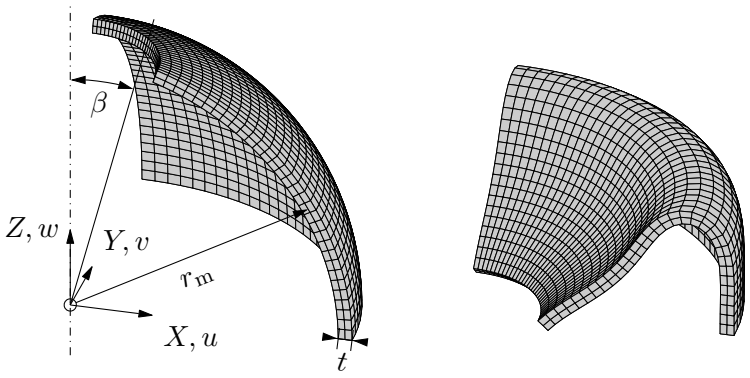

Figure 6: Spherical shell with opening: setup (left), deformed mesh (right).

of the used mesh is around 1, H1/P0ET6 exhibits pronounced robustness similar to H1/P0 (and H1/S18). The low reaction force R_z is explained by the too soft behavior of H1/P0ET6 for nearly undistorted meshes. All EAS elements require a much higher number of load steps as well as more than double the amount of NR iterations. We emphasize, that this behavior can not be observed for H1/P0ET6 if poor aspect ratios occur. In that case H1/P0ET6 performs extremely poor and even worse than EAS elements.[9]

[9] The convergence test of a circular ring (see e.g. Pfefferkorn et al. [9]) provides a good example of the poor behavior of H1/P0ET6 in shell-like problems.

Table 1: Results of the spherical shell test

element type	req. n_{steps}	total n_{NR}	R_z
H1/ET9	9	77	5487.5
H1/ET9-MIP	8	58	5487.5
HA1/ET12	9	77	5489.8
HA1/ET12-MIP	8	58	5489.8
H1/P0	3	27	5773.5
H1/P0ET6	3	29	4920.6
H1/S18	3	27	5454.1

4 Conclusion

The present paper covers the mixed pressure EAS element formulation of Armero [1] with an extension to 3D as well as thorough evaluation of the performance of the element regarding numerical instabilities such as spurious hourglassing patterns as well as locking and robustness in NR-iterations.

Although the element formulation of Armero [1] is stable and hourglassing-free for regular meshes with nonlinear elastic material behavior, some problems occur in case of distorted meshes and for elasto-plastic material behavior.

In particular, while Q1/P0ET2 solves the hourglass problems, that EAS element formulations such as Q1/ET4 suffer in case of 2D elasto-plastic simulations (see Armero [1]), converse results are observed in 3D computations. Here, H1/P0ET6 shows hourglassing and EAS elements show no spurious results.

In conclusion, there is yet an EAS based element formulation to be found, that is free of spurious hourglassing effects with nonlinear elastic and elasto-plastic material behavior in 2D and 3D, that furthermore provides the required robustness for different problem formulations. Finding such an element remains the task for element development. Nevertheless, the element formulation of Armero [1] provides an interesting mixed element with many desirable properties and works especially well in 2D.

References

[1] Armero, F. On the locking and stability of finite elements in finite deformation plane strain problems. In: *Computers and Structures*, 75(3): 261–290, 2000. doi: 10.1016/S0045-7949(99)00136-4.

[2] Boffi, D., Brezzi, F., and Fortin, M. *Mixed finite element methods and applications*. Heidelberg: Springer, 2013. doi: 10.1007/978-3-642-36519-5.

[3] Glaser, S. and Armero, F. On the formulation of enhanced strain finite elements in finite deformations. In: *Engineering Computations*, 14(7): 759–791, 1997. doi: 10.1108/02644409710188664.

[4] Hughes, T. *The finite element method: linear static and dynamic finite element analysis*. Mineola, NY: Dover Publ., 2000.

[5] Korelc, J., Šolinc, U., and Wriggers, P. An improved EAS brick element for finite deformation. In: *Computational Mechanics*, 46(4): 641–659, 2010. doi: 10.1007/s00466-010-0506-0.

[6] Korelc, J. and Wriggers, P. Consistent gradient formulation for a stable enhanced strain method for large deformations. In: *Engineering Computations*, 13(1): 641–659, 1996. doi: 10.1108/02644409610111001.

[7] Pfefferkorn, R. and Betsch, P. On transformations and shape functions for enhanced assumed strain elements. In: *International Journal for Numerical Methods in Engineering*, 120(2): 231–261, 2019. doi: 10.1002/nme.6133.

[8] Pfefferkorn, R. and Betsch, P. Extension of the enhanced assumed strain method based on the structure of polyconvex strain-energy functions. In: *International Journal for Numerical Methods in Engineering*, 121(8): 1695–1737, 2020. doi: 10.1002/nme.6284.

[9] Pfefferkorn, R., Bieber, S., Oesterle, B., Bischoff, M., and Betsch, P. Improving efficiency and robustness of EAS elements for nonlinear problems. In: *Int. J. Numer. Meth. Engng. (submitted)*, 2020.

[10] Pian, T. H. H. and Sumihara, K. Rational approach for assumed stress finite elements. In: *Int. J. Numer. Meth. Engng.*, 20(9): 1685–1695, 1984. doi: 10.1002/nme.1620200911.

[11] Simo, J. and Armero, F. Geometrically non-linear enhanced strain mixed methods and the method of incompatible modes. In: *International Journal for Numerical Methods in Engineering*, 33(7): 1413–1449, 1992. doi: 10.1002/nme.1620330705.

[12] Simo, J., Armero, F, and Taylor, R. Improved versions of assumed enhanced strain tri-linear elements for 3D finite deformation problems. In: *Computer Methods in Applied Mechanics and Engineering*, 110(3): 359–386, 1993. doi: 10.1016/0045-7825(93)90215-J.

[13] Simo, J. and Rifai, M. A class of mixed assumed strain methods and the method of incompatible modes. In: *International Journal for Numerical Methods in Engineering*, 29: 1595–1638, 1990. doi: 10.1002/nme.1620290802.

[14] Simo, J., Taylor, R., and Pister, K. variational and projection methods for the volume constraint in finite deformation elasto-plasticity. In: *Computer Methods in Applied Mechanics and Engineering*, 51: 177–208, 1985. doi: 10.1016/0045-7825(85)90033-7.

[15] Simo, J. C. Algorithms for static and dynamic multiplicative plasticity that preserve the classical return mapping schemes of the iInfinitesimal theory. In: *Comput. Methods Appl. Mech. Engrg.*, 99(1): 61–112, 1992. doi: 10.1016/0045-7825(92)90123-2.

[16] Viebahn, N., Schröder, J., and Wriggers, P. An extension of assumed stress finite elements to a general hyperelastic framework. In: *Advanced Modelling and Simulations in Engineering Science*, 6(9), 2019. doi: 10.1186/s40323-019-0133-z.

[17] Washizu, K. *variational methods in elasticity and plasticity*. Oxford: Pergamon press, 1975.

[18] Wilson, E., Taylor, R., Doherty, W., and Ghaboussi, J. Incompatible displacement models. In: *Numerical and Computer Methods in Structural Mechanics*. Ed. by S.J. Fenves, N. Perrone, A.R. Robinson, and W.C. Schnobrich. New York, 1973, pp. 43 –57. doi: 10.1016/B978-0-12-253250-4.50008-7.

[19] Wriggers, P. *Nonlinear finite element methods*. Berlin: Springer, 2008. doi: 10.1007/978-3-540-71001-1.

[20] Wriggers, P. and Reese, S. A note on enhanced strain methods for large deformations. In: *Computer Methods in Applied Mechanics and Engineering*, 135(3): 201 –209, 1996. doi: https://doi.org/10.1016/0045-7825(96)01037-7.